



This discussion paper is/has been under review for the journal The Cryosphere (TC).
Please refer to the corresponding final paper in TC if available.

TCD

5, 1921–1948, 2011

An improved
semi-empirical model

S. R. M. Ligtenberg et al.

An improved semi-empirical model for the densification of Antarctic firn

S. R. M. Ligtenberg, M. M. Helsen, and M. R. van den Broeke

Institute for Marine and Atmospheric research Utrecht (IMAU) P.O. Box 80000,
3508 TA Utrecht, The Netherlands

Received: 10 June 2011 – Accepted: 14 June 2011 – Published: 21 July 2011

Correspondence to: S. R. M. Ligtenberg (s.r.m.ligtenberg@uu.nl)

Published by Copernicus Publications on behalf of the European Geosciences Union.

Discussion Paper | Discussion Paper

Discussion Paper | Discussion Paper

Discussion Paper | Discussion Paper

[Title Page](#)

[Abstract](#)

[Introduction](#)

[Conclusions](#)

[References](#)

[Tables](#)

[Figures](#)

[◀](#)

[▶](#)

[◀](#)

[▶](#)

[Back](#)

[Close](#)

[Full Screen / Esc](#)

[Printer-friendly Version](#)

[Interactive Discussion](#)



Abstract

A firn densification model is presented that simulates steady-state Antarctic firn density profiles, as well as the temporal evolution of firn density and surface height. The model uses an improved firn densification expression that is tuned to fit depth-density observations. Liquid water processes (meltwater percolation, retention and refreezing) are also included. Two applications are presented. The steady-state model version is used to simulate the strong spatial variability in firn layer thickness across the Antarctic ice sheet. The time-dependent model is run for 3 Antarctic locations. It reveals a gentle upward motion of the surface during autumn, winter and spring, while during summer there is a more rapid lowering of the surface. Accumulation and (if present) melt introduce large inter-annual variability in surface height trends, possibly hiding ice dynamical thickening and thinning.

1 Introduction

The Antarctic ice sheet (AIS) is almost entirely covered by a layer of firn, the intermediate product in the transition from snow to ice. In Antarctica, fresh snow has a typical density of 350 kg m^{-3} , while glacier ice has a density of more than 900 kg m^{-3} . At low temperatures and accumulation rates, densification of firn is a slow process and the transition can take up to centuries or millennia. The large range of surface climate conditions in Antarctica introduces widely varying characteristics of the firn layer in space and time (Li and Zwally, 2004; van den Broeke, 2008; and Helsen et al., 2008). For instance, the firn layer thickness can vary between a few tens of meters in the relatively warm coastal areas to $>100 \text{ m}$ in the cold interior of East Antarctica. In ablation areas, where sublimation, snowdrift erosion and/or melt exceed snowfall, the firn layer can even be completely absent, resulting in formation of blue ice areas (Winther et al., 2001).

TCD

5, 1921–1948, 2011

An improved
semi-empirical model

S. R. M. Ligtenberg et al.

Title Page	
Abstract	Introduction
Conclusions	References
Tables	Figures
Discussion Paper	
◀	▶
◀	▶
Back	Close
Full Screen / Esc	
Printer-friendly Version	
Interactive Discussion	



An improved semi-empirical model

S. R. M. Ligtenberg et al.

[Title Page](#)[Abstract](#)[Introduction](#)[Conclusions](#)[References](#)[Tables](#)[Figures](#)[◀](#)[▶](#)[◀](#)[▶](#)[Back](#)[Close](#)[Full Screen / Esc](#)[Printer-friendly Version](#)[Interactive Discussion](#)

The steady and transient state of the firn layer provides important information on firn air content and surface elevation changes, which are crucial parameters to estimate the contemporary mass balance of the AIS using remote-sensing techniques (Rignot et al., 2008; Helsen et al., 2008; van den Broeke et al., 2008). Figure 1, adjusted from

5 Zwally and Li (2002), shows the various components of the vertical displacement of the ice sheet surface. A change in surface height with time (dH/dt) is given as the sum of these velocity components:

$$\frac{dH}{dt} = v_{\text{acc}} + v_{\text{me}} + v_{\text{fc}} + v_{\text{ice}} + v_{\text{b}} \quad (1)$$

where v_{acc} , v_{me} , v_{fc} , v_{ice} and v_{b} are the velocity components that represent accumulation, melt, firn compaction, ice flow and bedrock movement, respectively. Since we

10 focus on relatively short timescales, v_{b} is negligible and v_{ice} is assumed proportional to the average accumulation. The effect of sublimation is included in the accumulation

15 velocity, v_{acc} . These velocity components can be combined in time-dependent firn densification models to calculate temporal changes in firn depth and density and surface height changes, by forcing them with time series of surface temperature, snowfall,

sublimation and melt. These results can be used to convert satellite elevation change measurements to mass changes (Davis et al. (2005) and Wingham et al. (2009) among others). It has been demonstrated that variability in firn densification rate and accumulation strongly influence the observed surface height changes (Helsen et al. (2008);

20 McConnell et al., 2000).

Several models have been proposed to describe firn densification. Some are based on physical principles (for example Wilkinson, 1988), while others use semi-empirical parameterizations (Herron and Langway (1980); Barnola et al. (1991); Helsen et al. (2008), and Arthern et al., 2010). A distinction can also be made between models

25 that describe the steady-state density profile, and models that simulate changes in the firn layer over time. Steady-state firn profiles can be used to convert ice thickness to total mass of an ice column, the so-called firn correction. van den Broeke (2008) showed that the steady-state solution of Barnola et al. (1991) is in good agreement with

[Title Page](#)

[Abstract](#)

[Introduction](#)

[Conclusions](#)

[References](#)

[Tables](#)

[Figures](#)

[◀](#)

[▶](#)

[◀](#)

[▶](#)

[Back](#)

[Close](#)

[Full Screen / Esc](#)

[Printer-friendly Version](#)

[Interactive Discussion](#)



observations from firn cores, using regional atmospheric climate model output from van de Berg et al. (2006). For the upper layers, this model uses the semi-empirical steady-state solution of Herron and Langway (1980), while for the lower part the equations of Pimienta and Duval (1987) are used. Recent expressions for time-dependent firn densification and depth are those of Helsen et al. (2008) and Arthern et al. (2010), which are both based on the model of Herron and Langway (1980). The latter assumes that firn compaction has an Arrhenius-type temperature sensitivity and was tuned to fit steady-state density profiles from Greenland and Antarctica. A different temperature sensitivity was added by Li and Zwally (2004), which was later modified by Helsen et al. (2008) to make it suitable for Antarctica. None of these models included snow melt and refreezing, while it is well known that the higher density of refrozen melt water can have a significant effect on the density of the firn column and its densification rate.

In this paper we present a firn densification model (FDM) that calculates steady-state as well as time-dependent firn density profiles for Antarctica. The advantage of this model is that it uses the same densification expression for both purposes, tuned to optimally fit observations. Also snow melt and percolation, retention and refreezing of meltwater is implemented. In Sect. 2, we describe the model and its forcing. In Sect. 3, two applications are presented; first, we present an update of the characteristics and spatial variability of the steady-state Antarctic firn layer. Next, we present time series of surface height changes at various locations across Antarctica. For both applications, the FDM is forced with output of the regional atmospheric climate model RACMO2/ANT (Lenaerts et al., 2011a).

2 Methods

2.1 Atmospheric forcing

The FDM is forced at the surface by the surface mass balance, surface temperature and near-surface wind speed from the regional atmospheric climate model RACMO2/ANT.

[Title Page](#)[Abstract](#)[Introduction](#)[Conclusions](#)[References](#)[Tables](#)[Figures](#)[◀](#)[▶](#)[◀](#)[▶](#)[Back](#)[Close](#)[Full Screen / Esc](#)[Printer-friendly Version](#)[Interactive Discussion](#)

Model data is available for the period 1989–2009 at a temporal resolution of 6 h and a horizontal resolution of 27 km. RACMO2/ANT is forced at the lateral boundaries with ERA-Interim re-analysis data, which also provides the sea ice cover and sea surface temperatures. The average accumulation, as used in this paper, is the sum of solid

5 and liquid precipitation minus sublimation. The climate and surface mass balance of RACMO2/ANT has been validated by Lenaerts et al. (2011b); Lenaerts and van den Broeke (2011) and Kuipers Munneke et al. (2011) and is shown to provide a good representation of the Antarctic near-surface climate.

2.2 Firn densification model

10 Our FDM is a time-dependent one-dimensional model that keeps track of the density and temperature in a vertical firn column. For the density of new added surface snow, we use a parameterization of Kaspers et al. (2004), which is based on average accumulation (\dot{b}), near surface wind speed (\bar{V}_{10}) and surface temperature (\bar{T}_s), with a slope correction by Helsen et al. (2008):

$$15 \rho_s = -151.94 + 1.4266(73.6 + 1.06 \bar{T}_s + 0.0669 \dot{b} + 4.77 \bar{V}_{10}) \quad (2)$$

The previous model version (Helsen et al., 2008) did not consider processes associated with liquid water: rain, snow melt, percolation and refreezing. In the new model, these processes are implemented by allowing liquid water from rain and/or snowmelt to exist in – and move through – the firn column. Snowmelt is removed from the top layer,

20 and percolates down into the firn column. It refreezes when it reaches a firn layer with sufficient cold content ($T < 0^\circ\text{C}$) and pore space. To mimic capillary forces, a part of the liquid water remains in a layer that is at 0°C . The maximum amount of pore space used to store liquid water (W_{mi}) is taken as a function of the snow porosity P (Coléou and Lesaffre, 1998):

$$25 W_{mi} = 0.017 + 0.057 \left(\frac{P}{(1-P)} \right) \quad (3)$$

Typical values for W_{mi} are 0.09–0.13 close to the surface ($\rho = 300\text{--}400 \text{ kg m}^{-3}$) and 0.04 deeper in the firn column ($\rho \approx 650 \text{ kg m}^{-3}$). This retained water refreezes when the layer cools. By allowing water and therefore mass and heat to move through the firn column, the heat transport cannot be solved using an implicit numerical scheme, as in Helsen et al. (2008), but has to be solved explicitly, making the model computationally more expensive. The subsurface heat transport is simulated by using a one-dimensional time-dependent heat-transfer model (Paterson, 1994):

$$\frac{\delta T}{\delta t} = k \frac{\delta^2 T}{\delta z^2} \quad (4)$$

where k is the thermal diffusivity. This heat-transfer equation only contains a heat conduction term, where formally also heat advection and internal heating by deformation of ice should be included. However, the latter is small in the firn zone and therefore neglected, heat advection is implicitly taken into account by the downward motion of the firn layers at the speed of v_{ice} (Helsen et al., 2008).

The initial density profile of the time-dependent simulation is obtained by spinning up the model as long as needed to refresh the entire firn layer. As input the 1989–2009 period is extrapolated into a time series long enough for the spin-up period to be completed. Hence, we assume the 1989–2009 period is representative for the past 100–1000 years and the firn layer to be in steady state.

The previous model version used a densification expression adapted from Zwally and Li (2002), with a single densification expression for the complete density range. Various studies (Herron and Langway, 1980; Barnola et al., 1991) suggest one ($\rho \approx 550 \text{ kg m}^{-3}$) or even two ($\rho \approx 550 \text{ kg m}^{-3}$ and $\rho \approx 830 \text{ kg m}^{-3}$) critical values to separate different densification processes that occur in the firn column. In the upper part ($\rho \leq 550 \text{ kg m}^{-3}$), the dominant densification processes are grain settling and packing of snow grains (Herron and Langway, 1980). Thereafter, densification is slower and mainly due to sublimation, diffusion and deformation processes until the density reaches the pore close-off depth ($\rho \approx 830 \text{ kg m}^{-3}$), where the remaining air bubbles get

An improved semi-empirical model

S. R. M. Ligtenberg et al.

[Title Page](#)

[Abstract](#)

[Introduction](#)

[Conclusions](#)

[References](#)

[Tables](#)

[Figures](#)

[◀](#)

[▶](#)

[◀](#)

[▶](#)

[Back](#)

[Close](#)

[Full Screen / Esc](#)

[Printer-friendly Version](#)

[Interactive Discussion](#)



trapped in the ice. Further densification takes place by compression of these bubbles, until the density of glacier ice ($\rho \cong 910 \text{ kg m}^{-3}$) is reached.

Our FDM uses the dry snow densification expression proposed by Arthern et al. (2010) (Ar10 from now on) (Eq. 5). Ar10 use different densification expressions above and below the critical density value ($\rho = 550 \text{ kg m}^{-3}$) and therefore are better able to capture the faster densification near the surface.

$$\text{Ar10T: } \frac{d\rho}{dt} = C \dot{b} g (\rho_i - \rho) e^{(\frac{-E_c}{RT_s} + \frac{E_g}{RT_s})} \quad (5)$$

where E_c , E_g and C are constants, \dot{b} is the average accumulation, g the gravitational acceleration, ρ_i the ice density and R the gas constant and "T" in Ar10T refers to the time-dependent model version. Note that C has different values above (0.03) and below (0.07) the critical density level $\rho = 550 \text{ kg m}^{-3}$. To convert Ar10T to a steady-state solution (Ar10S), the vertical displacement of a firn layer has to equal the accumulation rate divided by the density. Also the local temperature (T_s) in the exponential term is replaced by the annual average surface temperature (\bar{T}_s):

$$\text{Ar10S: } \frac{d\rho}{dz} = C dz \rho g (\rho_i - \rho) e^{(\frac{-E_c}{RT_s} + \frac{E_g}{RT_s})} \quad (6)$$

where dz is the thickness of a firn layer. Figure 3a compares firn density profiles from Eq. 5 and 6 for a point in Marie Byrd Land (MBL), for which the climate characteristics are listed in Table 1. The oscillations in Ar10T are related to the strong non-linear dependence of densification rate on temperature. This effect is only present in the top few meters of the firn column, where the seasonal temperature cycle is significant. To compensate for this systematic bias and to enable a comparison with other steady-state models, an offset is applied to the surface density in the steady-state model, so that the critical $\rho = 550 \text{ kg m}^{-3}$ level occurs at the same depth in both solutions.

[Title Page](#)[Abstract](#)[Introduction](#)[Conclusions](#)[References](#)[Tables](#)[Figures](#)[|◀](#)[▶|](#)[◀](#)[▶](#)[Back](#)[Close](#)[Full Screen / Esc](#)[Printer-friendly Version](#)[Interactive Discussion](#)

2.3 Model performance and tuning

We compared the modelled depths of the critical density values $\rho = 550 \text{ kg m}^{-3}$ (z_{550}) and $\rho = 830 \text{ kg m}^{-3}$ (z_{830}) with observations from 48 ice core drilling sites in Antarctica (Fig. 2). We also compare the results of the steady-state model to van den Broeke (2008), who used the steady-state expressions of Barnola et al. (1991):

$$\text{Ba91 : } \begin{cases} \frac{d\rho}{dz} = 11 dz \rho (\rho_i - \rho) e^{\frac{-E}{RT_s}} & \text{for } \rho < 550 \text{ kg m}^{-3} \\ \frac{d\rho}{dz} = A_0 dz \rho \frac{t_{\text{yr}}}{b} f_e(\rho) \Delta P^3 e^{\frac{-E}{RT_s}} & \text{for } \rho > 550 \text{ kg m}^{-3} \end{cases} \quad (7)$$

where E and A_0 are constants, t_{yr} is the number of seconds in a year and ΔP the overburden pressure. Figure 3b compares the density profiles of Eq. 6 and 7 with the observed z_{550} and z_{830} at South Pole and MBL (climate characteristics are listed in Table 1). Although the densification expressions are quite different, the results for South Pole are similar and both correspond rather well with the observed depths. For the MBL point, Ba91 shows again good agreement with the observed depths, while Ar10S densifies too quickly and simulates too shallow depths. Around 15 m in the Ba91 simulation a numerical artifact is visible, caused by the overburden pressure ΔP in Eq. 7. Due to the shallow upper firn layer ($\rho \leq 550 \text{ kg m}^{-3}$) there is relatively little mass as overburden pressure, causing a lower densification rate above than below $\rho = 550 \text{ kg m}^{-3}$. However, Ba91 simulates the depths of the critical levels quite well.

Figure 4 compares observed and modelled z_{550} and z_{830} for all 48 observation locations. In order to isolate z_{830} from processes above z_{550} , we used $z_{830}^* = z_{830} - z_{550}$. Almost everywhere, Ar10S causes the firn to densify too quickly in the upper part of the firn column and therefore under-predicts z_{550} . The same pattern is observed for the points with a relatively small z_{830} , with deviations up to 50 %. However, for points with larger z_{830} the pattern is reversed. The Ba91 results are very similar to those of van den Broeke (2008), in which a previous RACMO2/ANT dataset (van de Berg et al., 2006) was used.

TCD

5, 1921–1948, 2011

An improved semi-empirical model

S. R. M. Ligtenberg et al.

[Title Page](#)

[Abstract](#)

[Introduction](#)

[Conclusions](#)

[References](#)

[Tables](#)

[Figures](#)

◀

▶

◀

▶

[Back](#)

[Close](#)

[Full Screen / Esc](#)

[Printer-friendly Version](#)

[Interactive Discussion](#)



The ratio of modelled to observed depths (MO) in Ar10S is found to be highly correlated with accumulation at the 48 core sites, both for z_{550} and z_{830} (Fig. 5). The correlation is such that the effect of the average accumulation \dot{b} on the densification rate is too large. Previously, Herron and Langway (1980) proposed the coefficient α in \dot{b}^α to be chosen between 0.5 and 1.1. However, Zwally and Li (2002) and Helsen et al. (2008) later assumed $\alpha = 1$. To introduce the correct accumulation dependence, we multiply the densification expressions of Ar10S with the relations of the regressions in Fig. 5, being:

$$MO_{550} = 1.415 - 0.147 \ln(\dot{b}) \quad \text{for } \rho < 550 \text{ kg m}^{-3} \quad (8)$$

$$MO_{830} = 2.335 - 0.288 \ln(\dot{b}) \quad \text{for } \rho > 550 \text{ kg m}^{-3} \quad (9)$$

For extreme accumulation values ($\dot{b} > 3322 \text{ mm yr}^{-1}$), MO_{830} becomes negative, which occurs on a few points in the Antarctic Peninsula. $MO_{550} = 0$ is not reached for realistic values of \dot{b} . We impose a minimum value of 0.25 on MO_{550} and MO_{830} , corresponding roughly to areas where accumulation exceeds 1400 mm yr^{-1} . Figure 6 compares the observed to the updated model values of z_{550} and z_{830} . For both critical depths, the agreement of the steady-state FDM with the observations is now comparable to Ba91, but the great advantage of the new expression is that it can also be used in a time-dependent fashion.

3 Applications

20 3.1 Steady-state Antarctic firn density profiles

The steady-state expression forced by average RACMO2/ANT climate fields of accumulation, surface temperature and wind speed, enables us to look at the spatial variability of the characteristics of the Antarctic firn column (Fig. 7 and 8). Since the resolution of RACMO2/ANT output has increased from 55 to 27 km, we see much more detail

An improved semi-empirical model

S. R. M. Ligtenberg et al.

[Title Page](#)

[Abstract](#)

[Introduction](#)

[Conclusions](#)

[References](#)

[Tables](#)

[Figures](#)

[◀](#)

[▶](#)

[◀](#)

[▶](#)

[Back](#)

[Close](#)

[Full Screen / Esc](#)

[Printer-friendly Version](#)

[Interactive Discussion](#)



than in van den Broeke (2008). The modelled density of the surface snow is shown in Fig. 7a and shows a typical distribution of relatively low density surface snow in the East Antarctic interior ($300\text{--}340\text{ kg m}^{-3}$), and high densities along the ice sheet margin ($420\text{--}460\text{ kg m}^{-3}$), where temperature, precipitation and wind speeds are high. The two large ice shelves have a slightly lower surface density than other coastal regions because, in absence of orographic forcing, the accumulation is relatively small. Along the West Antarctic coast and in the Antarctic Peninsula, the highest surface density values occur, forced by a combination of high temperatures, wind speeds and precipitation rates.

The points without values in Figs. 7 and 8 are regions where, according to RACMO2/ANT, no stable firn layer can exist as accumulation (1989–2009) is exceeded by either sublimation or melt. The location of these so called blue ice areas correspond reasonably well to the areas presented in Winther et al. (2001). Wind-induced blue ice areas occur in the vicinity of the Lambert Glacier and along the eastern border of the Transantarctic Mountains. On Larsen C Ice Shelf, snow melt exceeds precipitation in RACMO2/ANT, so no long-term firn layer can build up. As Larsen C is currently covered by a significant layer of firn (Holland et al., 2011), it is likely that the present firn layer was formed before the recent warming of the Antarctic Peninsula (Vaughan et al., 2003) and is now slowly degrading.

Figures 7b-c show the spatial distribution of two critical depths in the firn column; z_{550} and z_{830} . These fields show roughly the inverse pattern of surface density. This is especially valid for z_{550} as the surface density (ranging from 300 kg m^{-3} to 450 kg m^{-3}) determines the start of the density-depth profile. The highest values of z_{550} and z_{830} are found in the interior of East Antarctica with smaller values in the coastal regions.

In West Antarctica and the Antarctic Peninsula the pattern is somewhat different; z_{830} shows relatively high values while z_{550} is small. This is caused by the high accumulation values in these regions, the fast burial of fresh snow leads to a slow densification with depth. The thickness of the firn column, taken as z_{830} , is only 40–50 m around and on the big ice shelves (Ross Ice Shelf, Filchner Ronne Ice Shelf and the Amery

Ice Shelf). Here, a combination of relatively high temperatures and relatively low precipitation amounts cause a rapid densification of the firn with depth. The highest values are found along the crest of the plateau with values just reaching 120 m.

TCD

5, 1921–1948, 2011

An important quantity is the amount of air in the firn column. The thickness change resulting from compressing the whole firn column until it has ice density gives the amount of air, also called the firn-depth correction. Figure 8a shows the spatial distribution of the firn depth correction. It resembles the depth of the firn layer in Fig. 7c, indicating that deeper firn columns generally contain more air than shallow columns. This is supported by the average density of the firn column, which shows little variability; values range between 650 kg m^{-3} on the East Antarctic plateau to 690 kg m^{-3} along the edges of the ice sheet (not shown). On average there is 22.6 m of air in the firn column, but the modelled range of values is large (10–40 m), due the previously mentioned climatic differences between the coastal regions and the interior. The average thickness of the Antarctic ice sheet is 2.06 km (Lythe et al., 2001), so on average a firn depth correction of just over 1 % has to be applied to get the total mass of the ice sheet. However, ice thicknesses are smaller near the coast; here, the firn correction can be significant, especially when it is used to derive ice thickness of floating glacier tongues, using surface elevation in combination with a floatation criterium (van den Broeke et al. (2008); Rignot et al. (2008)). Figure 8b expresses the air thickness as a percentage of the total ice column. On the ice shelves and in coastal and mountainous areas, values of 7–9 % are found. White areas indicate BEDMAP ice thicknesses that were shallower than the modelled firn-ice transition depths.

3.2 Time-dependent firn density and surface elevation

By forcing the time-dependent FDM with model time series, we obtain the evolution of the surface height with time, so that the individual processes that contribute to the vertical movement of the surface can be examined. Fig. 9a–c shows the seasonal cycle of the surface velocity components and Fig. 9d–f the resulting surface elevation evolution, i.e. the integrated signal of v_{tot} in Fig. 9a–c, for three locations on the AIS

An improved semi-empirical model

S. R. M. Ligtenberg et al.

[Title Page](#)

[Abstract](#)

[Introduction](#)

[Conclusions](#)

[References](#)

[Tables](#)

[Figures](#)

◀

▶

◀

▶

[Back](#)

[Close](#)

[Full Screen / Esc](#)

[Printer-friendly Version](#)

[Interactive Discussion](#)



(Fig. 2): P1 is located in the cold and dry East Antarctic interior, P2 is in wetter and warmer West Antarctica and P3 in coastal Dronning Maud Land where significant melt occurs. The climate characteristics of these points are shown in Table 2:

The average seasonal cycle is similar for the three locations, with upward motion of the surface (positive v_{tot}) in autumn, winter and spring and a relatively strong downward motion (negative v_{tot}) in summer. At all three locations, v_{ice} is constant throughout the year, as it is assumed proportional to the average accumulation. At P1 and P2, no melt occurs ($v_{\text{melt}} = 0$), hence the seasonal variations are determined by accumulation and firn densification. The strong non-linear temperature dependence of the latter causes a densification peak in summer. In combination with a summer minimum in v_{acc} , this causes the summer lowering of the surface. The contribution of firn densification to the vertical movement of the surface is relatively constant from year to year, as only the upper few meters of the firn layer experience significant annual temperature changes. So, at P1 and P2, the variations in v_{total} are mainly caused by variability in snowfall.

At P3, melt mainly occurs in December and January, which lowers the surface significantly. In combination with the variability in accumulation, this leads to a relatively large inter-annual variability for the summer months. Interestingly, the contribution to surface lowering by firn densification is almost three times smaller at P3 than at P2. One reason is the presence of refrozen meltwater in the firn column at P3, which causes higher average firn densities and therefore limits the potential total firn densification. Also, the firn layer at P2 is much deeper than at P3, due to the higher accumulation amounts.

Figure 10 shows the surface height evolution for the entire 21-year period (1989–2009) at P2 and P3. The evolution of the surface height in P1 shows small inter-annual variability and is therefore not included. For P2 and P3, the inter-annual variability as discussed above is visible as decadal trends. At P2, inter-annual variability is almost completely caused by accumulation variability where wetter (e.g. 2005–2006) and dryer (1995–1998) than average periods cause upward or downward trends in surface height. An interesting asymmetry is visible: the lowering at P2 is more gentle than in P3, as firn densification is a slow, but steady process compared to melt. At

[Title Page](#)[Abstract](#)[Introduction](#)[Conclusions](#)[References](#)[Tables](#)[Figures](#)[◀](#)[▶](#)[◀](#)[▶](#)[Back](#)[Close](#)[Full Screen / Esc](#)[Printer-friendly Version](#)[Interactive Discussion](#)

P3, rapid lowering of the surface is mainly caused by strong melt seasons (e.g. 1997–1998), while upward motions are associated with wetter periods or a weak melt season (e.g. 2008–2009).

TCD

5, 1921–1948, 2011

4 Summary and conclusions

5 After introducing an accumulation dependence into the Ar10 densification expression, good agreement is found with 48 steady-state firn profiles from the Antarctic ice sheet. The steady-state version of the new densification expression produces results comparable to the steady-state solution of Barnola et al. (1991). A great advantage of the updated expression is that it can also be used in time-dependent mode. Moreover, by
10 introducing liquid water into the model, it can now be applied to the entire Antarctic ice sheet including its floating ice shelves, as long as the surface mass balance is positive and a firn layer can build up.

In steady-state mode, the FDM is used to assess the spatially variable characteristics of the Antarctic firn layer. On the cold and dry East Antarctic plateau, the lowest
15 surface snow density and deepest firn-ice transitions are found. Moving towards the coastal areas the climate gets warmer, wetter and windier, causing the surface density to increase and the firn layer depth to decrease. Some regions do not obey this general pattern, e.g. the coast of West Antarctica shows high surface densities and small values of the depth of the $\rho = 550 \text{ kg m}^{-3}$ level (z_{550}), but deep firn-ice transition depths (z_{830}), reaching 120 m. This is caused by the high accumulation rates that decrease the average densification rate with depth. The same effect occurs along the
20 Antarctic mountain ranges, but is less outspoken and only present in some isolated spots. Steady-state profiles can be used to quantify the firn-depth correction, a quantity needed to convert ice thickness to total ice mass. The firn correction averaged over the entire ice sheet is small (1 %), but along mountain ranges and especially on ice shelves, the values go up to 9 %. This constitutes a significant correction for ice flux calculations at the grounding line (e.g. Rignot et al., 2008). The spatial variability of
25

Discussion Paper

Discussion Paper

Discussion Paper

Discussion Paper

An improved semi-empirical model

S. R. M. Ligtenberg et al.

[Title Page](#)

[Abstract](#)

[Introduction](#)

[Conclusions](#)

[References](#)

[Tables](#)

[Figures](#)

◀

▶

◀

▶

[Back](#)

[Close](#)

[Full Screen / Esc](#)

[Printer-friendly Version](#)

[Interactive Discussion](#)



firn layer characteristics resembles that presented by van den Broeke (2008), but with much improved horizontal resolution.

The effect of melt is not included in the steady-state profiles: if melt occurs, melt-water refreezes deeper in the firn column resulting in layers with higher density and/or complete ice lenses. In a steady-state profile these features cannot be modelled, as they move to greater depths with time. On average, the density will be higher due to this refrozen water. As heat is released upon refreezing, the local firn temperature will increase, further accelerating the densification. On the other hand, ice layers lead to a higher average density, which in turn decreases the potential densification rate.

The time-dependent version of the FDM is used to study the evolution of the surface height and firn density in time and depth. It shows that everywhere in Antarctica, the surface elevation shows a clear annual cycle with upward motion in austral autumn, winter and spring due to accumulation and relatively slow firn compaction, and a lowering in summer when accumulation is lower and firn densification is more rapid in response to higher temperatures. If melt is present, the lowering of the surface in summer is even more pronounced. In the interior of Antarctica, the year-to-year surface elevation variability is almost completely caused by the variability in accumulation, while in melt areas the strength of the melt season is also important. Firn densification rate shows less year-to-year variability.

References

Arthern, R. J., Vaughan, D. G., Rankin, A. M., Mulvaney, R., and Thomas, E. R.: In situ measurements of Antarctic snow compaction compared with predictions of models, *J. Geophys. Res.*, 115, (F03011), doi:10.1029/2009JF001306, 2010. 1923, 1924, 1927

Barnola, J.-M., Pimienta, P., Raynaud, D., and Korotkevich, Y. S.: CO₂-climate relationship as deduced from the Vostok ice core: a re-examination based on new measurements and on a re-evaluation of the air dating, *Tellus*, 43B, 83–90, 1991. 1923, 1926, 1928, 1933

Coléou, C. and Lesaffre, B.: Irreducible water saturation in snow: experimental results in a cold laboratory, *Ann. Glaciol.*, 26, 64–68, 1998. 1925

[Title Page](#)

[Abstract](#)

[Introduction](#)

[Conclusions](#)

[References](#)

[Tables](#)

[Figures](#)

[◀](#)

[▶](#)

[◀](#)

[▶](#)

[Back](#)

[Close](#)

[Full Screen / Esc](#)

[Printer-friendly Version](#)

[Interactive Discussion](#)



Davis, C. H., Li, Y., McConnell, J. R., Frey, M. M., and Hanna, E.: Snowfall-driven growth in East Antarctic ice sheet mitigates recent sea-level rise, *Science*, 308, 1898–1901, doi:10.1126/science.1110662, 2005. 1923

Helsen, M., M. R. van den Broeke, R. S. W. van de Wal, W. J. van de Berg, E. van Meijgaard, C. H. Davis, Y. Li, and I. Goodwin (2008), Elevation changes in Antarctica mainly determined by accumulation variability, *Science*, 320, 1626–1628, doi:10.1126/science.1153894. 1922, 1923, 1924, 1925, 1926, 1929

Herron, M. and Langway, C.: Firn densification: an empirical model, *J. Glaciol.*, 25(93), 373–385, 1980. 1923, 1924, 1926, 1929

Holland, P. R., Corr, H. F. J., Pritchard, H. D., Vaughan, D. G., Arthern, R. J., Jenkins, A., and Tedesco, M.: The air content of Larsen C ice shelf, *Geophys. Res. Lett.*, 38, L10503, doi:10.1029/2011GL047245, 2011. 1930

Kaspers, K. A., van de Wal, R. S. W., van den Broeke, M. R., Schwander, J., van Lipzig, N. P. M., and Brenninkmeijer, C. A. M.: Model calculations of the age of firn air across the Antarctic continent, *Atmos. Chem. Phys. Discuss.*, 4, 1817–1853, doi:10.5194/acpd-4-1817-2004, 2004. 1925

Kuipers Munneke, P., van den Broeke, M. R., Lenaerts, J. T. M., Flanner, M. G., Gardner, A. S., and van de Berg, W. J.: A new albedo parameterization for use in climate models over the Antarctic ice sheet, *J. Geophys. Res.*, 116, D05114, doi:10.1029/2010JD015113, 2011. 1925

Lenaerts, J. T. M. and van den Broeke, M. R.: Modeling snowdrift in Antarctica with a regional climate model, Part II: Results, *J. Geophys. Res.*, in review, 2011. 1925

Lenaerts, J. T. M., van den Broeke, M. R., van de Berg, W. J., van Meijgaard, E., and Munneke, P. K.: A new, high resolution surface mass balance map of antarctica (1989–2009) based on regional climate modeling, *Geophys. Res. Lett.*, in review, (2011a). 1924

Lenaerts, J. T. M., van den Broeke, M. R., Déry, S. J., van Meijgaard, E., van de Berg, W. J., Palm, S. P., and Rodrigo, J. S.: Modeling snowdrift in Antarctica with a regional climate model, Part I: Methods and model evaluation, *J. Geophys. Res.*, in review, (2011b). 1925

Li, J., and Zwally, H. J.: Modeling the density variation in the shallow firn layer, *Ann. Glaciol.*, 38, 303–313, 2004. 1922, 1924

Lythe, M. B., Vaughan, D. G., and the BEDMAP Consortium BEDMAP: A new ice thickness and subglacial topographic model of Antarctica, *J. Geophys. Res.*, 106(B6), 11335–11352, doi:10.1029/2000JB900449, 2001. 1931

An improved semi-empirical model

S. R. M. Ligtenberg et al.

[Title Page](#)

[Abstract](#)

[Introduction](#)

[Conclusions](#)

[References](#)

[Tables](#)

[Figures](#)

◀

▶

◀

▶

[Back](#)

[Close](#)

[Full Screen / Esc](#)

[Printer-friendly Version](#)

[Interactive Discussion](#)



McConnell, J. R., Arthern, R. J., Mosley-Thompson, E., Davis, C. H., Bales, R. C., Thomas, R., Burkhardt, J. F., and Kyne, J. D.: Changes in Greenland ice sheet elevation attributed primarily to snow accumulation variability, *Nature*, 406, 877–879, 2000. 1923

Paterson, W. S. B.: The physics of glaciers, 3 Edn., Pergamon, 1994. 1926

5 Pimenta, M. and Duval, P.: Rate controlling processes in the creep of polar glacier ice, *J. Phys.*, 48, 243–248, 1987. 1924

Rignot, E., Bamber, J. L., van den Broeke, M. R., Davis, C., Li, Y., van de Berg, W. J., and van Meijgaard, E.: Recent Antarctic ice mass loss from radar interferometry and regional climate modelling, *Nat. Geosci.*, 1, 106–110, doi:10.1038/ngeo102, 2008. 1923, 1931, 1933

10 van de Berg, W. J., van den Broeke, M. R., Reijmer, C. H., and van Meijgaard, E.: Reassessment of the Antarctic surface mass balance using calibrated output of a regional atmospheric climate model, *J. Geophys. Res.*, 111, (D11104), doi:10.1029/2005JD006495, 2006. 1924, 1928

van den Broeke, M. R.: Depth and density of the Antarctic firn layer, *Arctic, Antarct. Alp. Res.*, 40(2), 432–438, 10.1657/1523-0430(07-021)[BROEKE]2.0.CO;2, 2008. 1922, 1923, 1928, 15 1930, 1934

van den Broeke, M. R., van de Berg, W. J., and van Meijgaard, E.: Firn depth correction along the Antarctic grounding line, *Antarct. Sci.*, 20, 513–517, doi:10.1017/S095410200800148X, 2008. 1923, 1931

20 Vaughan, D. G., Marshall, G. J., Connolley, W. M., Parkinson, C., Mulvaney, R., Hodgson, D. A., King, J. C., Pudsey, C. J., and Turner, J.: Recent rapid regional climate warming on the Antarctic Peninsula, *Climate Change*, 60(3), 243–274, doi:10.1023/A:1026021217991, 2003. 1930

Wilkinson, D. S.: A pressure-sintering model for the densification of polar firn and glacier ice, *J. Glaciol.*, 34(116), 40–45, 1988. 1923

25 Wingham, D. J., Wallis, D. W., and Shepherd, A.: Spatial and temporal evolution of Pine Island Glacier thinning, *Geophys. Res. Lett.*, 36, L17501, doi:10.1029/2009GL039126, 2009. 1923

Winther, J.-G., Jespersen, M. N., and Liston, G. E.: Blue-ice areas in Antarctica derived from NOAA AVHRR satellite data, *J. Glaciol.*, 47(157), 325–334, 2001. 1922, 1930

30 Zwally, H. J. and Li, J.: Seasonal and interannual variations of firn densification and ice-sheet surface elevation at the Greenland Summit, *J. Glaciol.*, 48(161), 199–207, doi:10.3189/172756502781831403, 2002. 1923, 1926, 1929, 1939

An improved semi-empirical model

S. R. M. Ligtenberg et al.

[Title Page](#)

[Abstract](#)

[Introduction](#)

[Conclusions](#)

[References](#)

[Tables](#)

[Figures](#)

◀

▶

◀

▶

[Back](#)

[Close](#)

[Full Screen / Esc](#)

[Printer-friendly Version](#)

[Interactive Discussion](#)



An improved
semi-empirical model

S. R. M. Ligtenberg et al.

Table 1. RACMO2/ANT climate characteristics of a point in Marie Byrd Land and South Pole: latitude, longitude, height above sea level, average annual temperature, accumulation, 10 m wind speed and melt over the 1989–2009 period.

	Lat (°N)	Lon (°E)	h_s (m)	\bar{T}_s (K)	\dot{b} (mm yr $^{-1}$)	\bar{V}_{10} (m s $^{-1}$)	\bar{M} (mm yr $^{-1}$)
MBL	−79.6	105.0	1912	240.8	319.8	6.58	0.0
SP	−90.0	0.0	2797	220.7	55.9	5.61	0.0

[Title Page](#)[Abstract](#)[Introduction](#)[Conclusions](#)[References](#)[Tables](#)[Figures](#)[|◀](#)[▶|](#)[◀](#)[▶](#)[Back](#)[Close](#)[Full Screen / Esc](#)[Printer-friendly Version](#)[Interactive Discussion](#)

An improved
semi-empirical model

S. R. M. Ligtenberg et al.

Table 2. RACMO2/ANT climate characteristics of points P1, P2 and P3: latitude, longitude, height above sea level, average annual temperature, accumulation, 10 m wind speed and melt over the 1989–2009 period.

	Lat (°N)	Lon (°E)	h_s (m)	\bar{T}_s (K)	\dot{b} (mm yr ⁻¹)	\bar{V}_{10} (m s ⁻¹)	\bar{M} (mm yr ⁻¹)
P1	-75.1	123.4	3262	217.8	18.0	4.79	0.0
P2	-77.8	-102.9	1392	245.7	518.8	7.14	0.0
P3	-71.1	-10.9	40	256.0	276.4	8.30	51.2

[Title Page](#)[Abstract](#)[Introduction](#)[Conclusions](#)[References](#)[Tables](#)[Figures](#)[◀](#)[▶](#)[◀](#)[▶](#)[Back](#)[Close](#)[Full Screen / Esc](#)[Printer-friendly Version](#)[Interactive Discussion](#)

An improved
semi-empirical model

S. R. M. Ligtenberg et al.

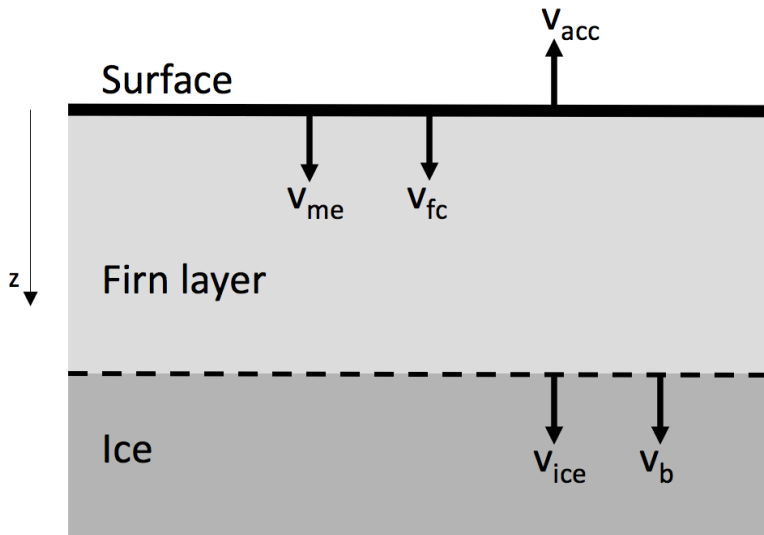


Fig. 1. Velocity components contributing to surface elevation changes: accumulation (v_{acc}), melt (v_{me}), firn compaction (v_{fc}), downward ice flow (v_{ice}) and bedrock movement (v_b), adjusted from Zwally and Li (2002).

An improved
semi-empirical model

S. R. M. Ligtenberg et al.

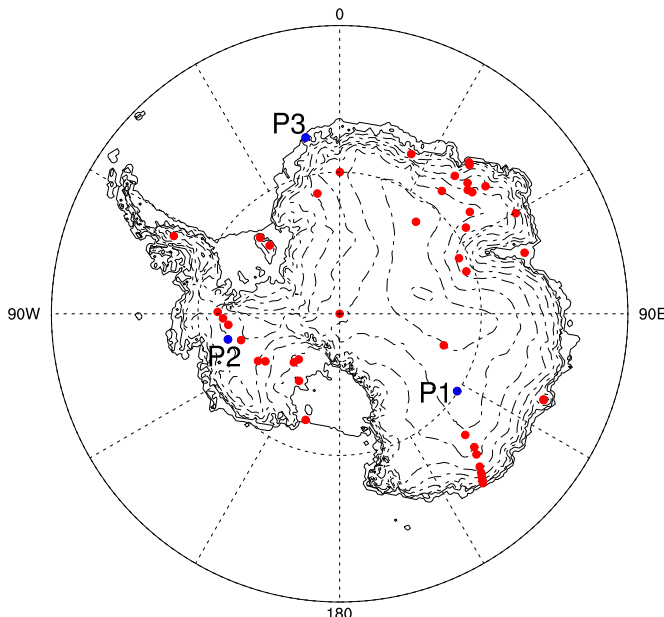


Fig. 2. Locations of 48 firn cores used in the model comparison in Sect. 2 (red and blue) and the locations of P1, P2 and P3, used in the analysis in Sect. 3.2 (blue).

[Title Page](#)[Abstract](#)[Introduction](#)[Conclusions](#)[References](#)[Tables](#)[Figures](#)[|◀](#)[▶|](#)[◀](#)[▶](#)[Back](#)[Close](#)[Full Screen / Esc](#)[Printer-friendly Version](#)[Interactive Discussion](#)

An improved semi-empirical model

S. R. M. Ligtenberg et al.

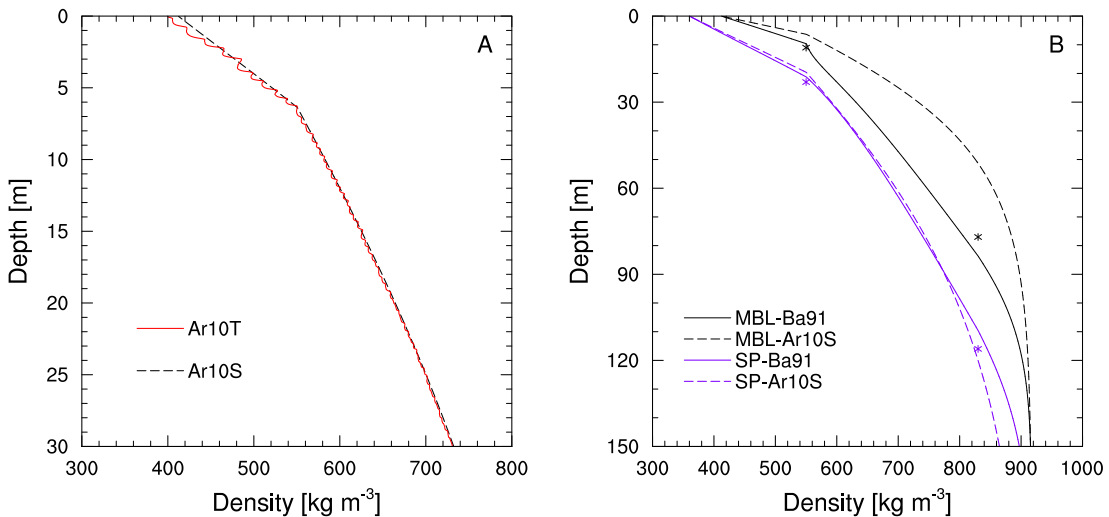


Fig. 3. Firn density profiles of the steady-state Ar10S and time-dependent Ar10T densification expressions for a location in Marie Byrd Land **(A)** and steady-state density profiles of Ar10S and Ba91, with the observed z_{550} and z_{830} **(B)** for South Pole (purple) and the MBL location as in Fig. A (black). Climatic characteristics of both points are listed in Table 1.

[Title Page](#)[Abstract](#)[Introduction](#)[Conclusions](#)[References](#)[Tables](#)[Figures](#)[|◀](#)[▶|](#)[◀](#)[▶](#)[Back](#)[Close](#)[Full Screen / Esc](#)[Printer-friendly Version](#)[Interactive Discussion](#)

An improved semi-empirical model

S. R. M. Ligtenberg et al.

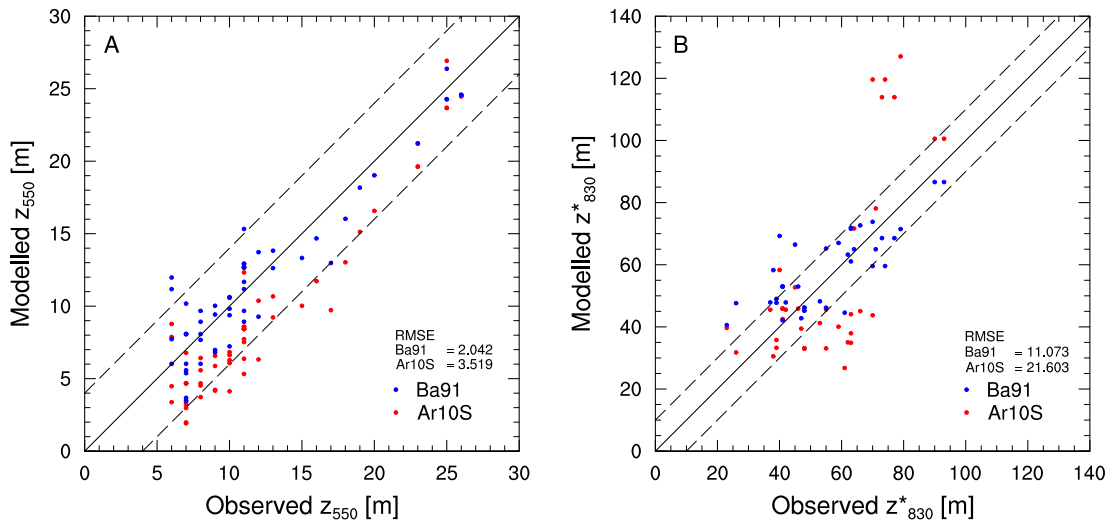


Fig. 4. Modelled vs observed depth of the $\rho = 550 \text{ kg m}^{-3}$ (**A**) and $\rho = 830 \text{ kg m}^{-3}$ (**B**) levels, for the densification expressions of Ar10S and Ba91.

[Title Page](#) [Abstract](#) [Introduction](#)
[Conclusions](#) [References](#)
[Tables](#) [Figures](#)

[◀](#) [▶](#)
[◀](#) [▶](#)
[Back](#) [Close](#)
[Full Screen / Esc](#)

[Printer-friendly Version](#)
[Interactive Discussion](#)



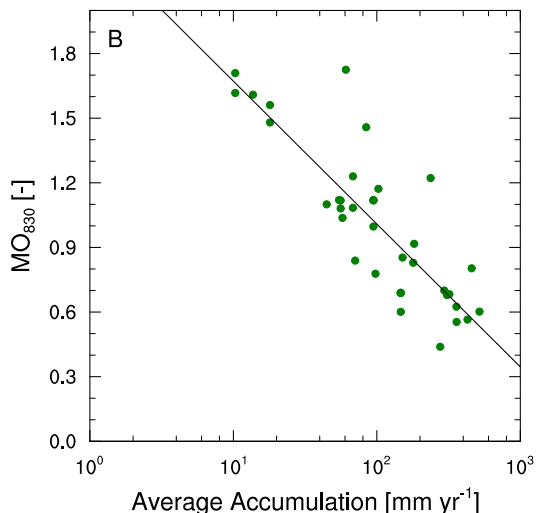


Fig. 5. MO-ratio of Ar10S for z_{550} (**A**) and z_{830}^* (**B**) vs. the average accumulation, the regression line equations are listed in Eq. 8 and 9.

Fig. 6. Modelled vs observed depth of the $\rho = 550 \text{ kg m}^{-3}$ **(A)** and $\rho = 830 \text{ kg m}^{-3}$ **(B)** levels, for the updated densification expressions of Ar10S and Ba91.

Title Page

Abstract

Introduction

Conclusion

References

Tables

Figures

1

▶

1

1

Back

Close

Full Screen / Esc

Interactive Discussion



An improved semi-empirical model

S. R. M. Ligtenberg et al.

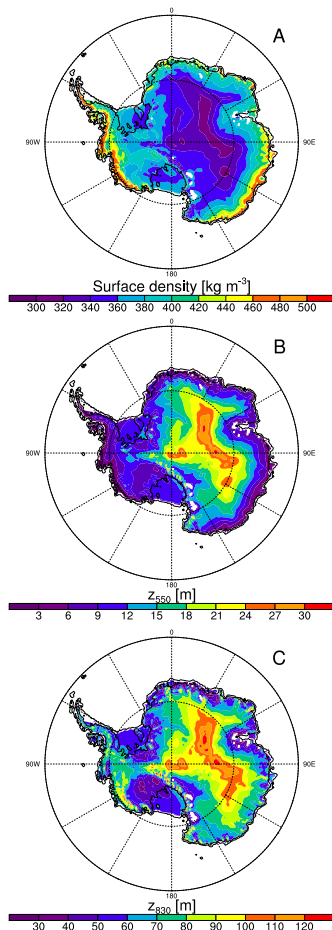


Fig. 7. Modelled surface density (**A**) and depths of the critical density levels $\rho = 550 \text{ kg m}^{-3}$ (**B**) and $\rho = 830 \text{ kg m}^{-3}$ (**C**).

[Title Page](#)[Abstract](#)[Introduction](#)[Conclusions](#)[References](#)[Tables](#)[Figures](#)[|◀](#)[▶|](#)[◀](#)[▶](#)[Back](#)[Close](#)[Full Screen / Esc](#)[Printer-friendly Version](#)[Interactive Discussion](#)

An improved
semi-empirical model

S. R. M. Ligtenberg et al.

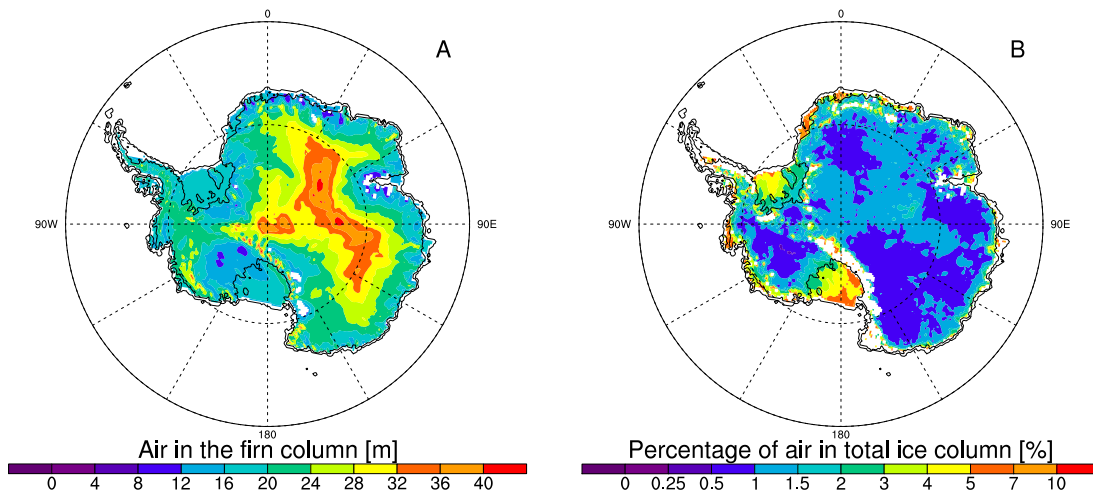


Fig. 8. The modelled amount of air in the firn column, expressed as the firn correction in m (**A**) and as a fraction of the total thickness of the ice in % (**B**).

[Title Page](#)[Abstract](#)[Introduction](#)[Conclusions](#)[References](#)[Tables](#)[Figures](#)[|◀](#)[▶|](#)[◀](#)[▶](#)[Back](#)[Close](#)[Full Screen / Esc](#)[Printer-friendly Version](#)[Interactive Discussion](#)

An improved
semi-empirical model

S. R. M. Ligtenberg et al.

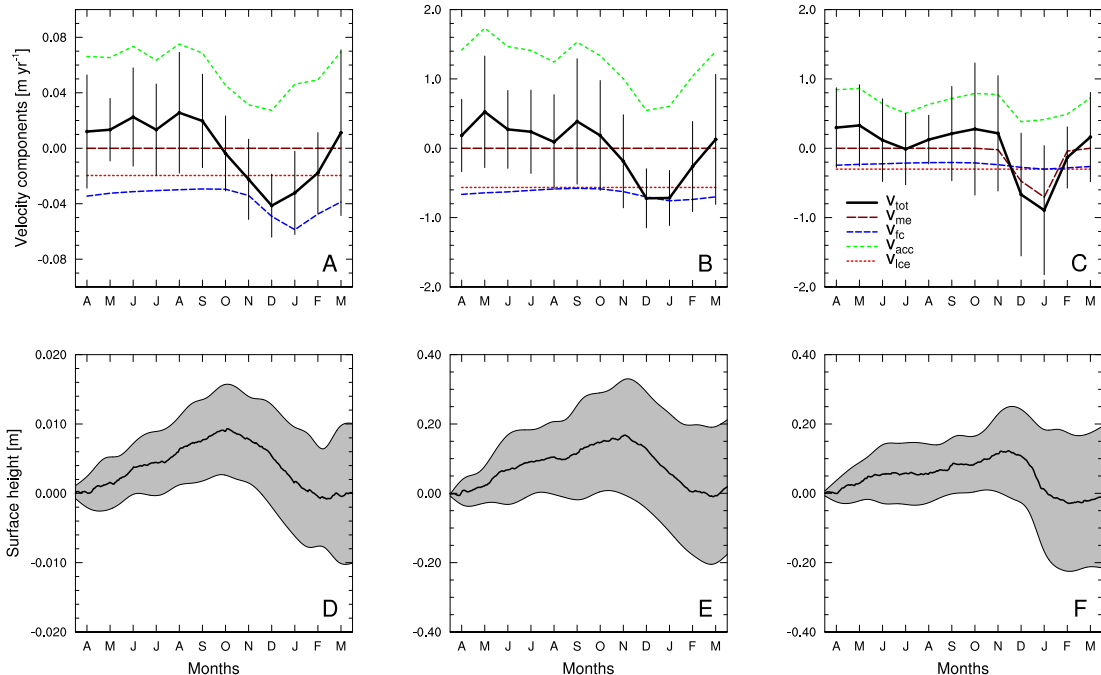


Fig. 9. The monthly averaged (1989–2009) velocity components that determine the vertical displacement of the surface: v_{acc} , v_{me} , v_{fc} , v_{ice} and v_{total} (**A**, **B**, **C**) and the daily averaged (1989–2009) surface height and standard deviation (**D**, **E**, **F**) for P1, P2 and P3 (see Fig. 2). Note the different scales.

Title Page

Abstract

Introduction

Conclusions

References

Tables

Figures

◀

▶

◀

▶

Back

Close

Full Screen / Esc

Printer-friendly Version

Interactive Discussion



An improved
semi-empirical model

S. R. M. Ligtenberg et al.

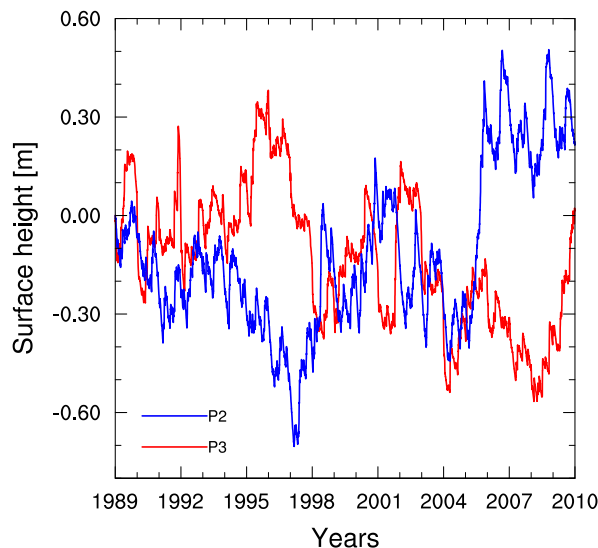
[Title Page](#)[Abstract](#)[Introduction](#)[Conclusions](#)[References](#)[Tables](#)[Figures](#)[|◀](#)[▶|](#)[◀](#)[▶](#)[Back](#)[Close](#)[Full Screen / Esc](#)[Printer-friendly Version](#)[Interactive Discussion](#)

Fig. 10. Surface height evolution (1989–2009) for P2 and P3 (see Fig. 2).